

# FLOW FORMABILITY OF ALUMINUM ALLOYS FOR AEROSPACE INTEGRALLY STIFFENED CYLINDERS

Mary Cecilia Mulvaney, *PhD Candidate*, University of Virginia  
James M. Fitz-Gerald, *Advisor*, University of Virginia

## Abstract

Flow forming of aluminum (Al) integrally stiffened cylinders (ISCs) for aerospace structures is currently limited by the available alloys that can sustain the severe plastic deformation inherent to the process. In this investigation, three commercial Al alloys (designated 6061, 2139, and 5083) were subjected to tensile testing and forming trials to identify mechanical properties that best predict spin and flow formability. Al 6061 performed best in the forming trials by conforming with the final part geometry, which was consistent with high total elongation and percent area reduction during tensile testing. In contrast, Al 2139 and Al 5083 both failed during the third of five spin forming passes, likely due to lower total elongation and percent area reduction values. Al 2139 and Al 5083 did exhibit higher strength, modulus of resilience, and fracture toughness than Al 6061. These findings emphasize the importance of improving the formability of Al 2139 and Al 5083 to produce fully formed parts with mechanical properties superior to Al 6061.

## Introduction

### Motivation

The integrally stiffened cylinder (ISC) process is poised to significantly reduce the manufacturing time and increase the structural efficiency of a number of aerospace structures. Originally developed for launch vehicle cryogenic tanks, the ISC process utilizes flow forming to create longitudinal stiffeners that are integral to the outer skin<sup>[1]</sup>. A NASA study showed that fabricating rocket structures with ISCs would lead to a 7% or greater reduction in mass and a 50% cost and schedule reduction due to time savings in minimizing the machining, welding, and inspection the multi-piece tanks<sup>[2]</sup>. Similar benefits are expected for aircraft fuselages constructed from ISCs, where tens of thousands of rivets joining stiffeners to aircraft skins could be eliminated by the ISC process<sup>[1]</sup>.

The flow forming success of ISCs has been shown to depend on the Al alloy selected. Prior work at the 3 m diameter scale has revealed that common aerospace alloys, such as Al 2219, can crack during flow forming, severely limiting the utility of high strength alloys for ISCs<sup>[3]</sup>. Furthermore, such alloys require multi-step heat treatments to achieve acceptable service properties, adding time and the risk of distortion to ISC fabrication. Purely work hardenable Al alloys (the 5xxx-series) may be candidate ISC materials since

they develop strength through deformation rather than heat treatment. Prior work has shown that the Al-2.5Mg alloy 5052 exhibited good ambient temperature flow formability and higher as-formed properties compared to the highly formable alloy 6061<sup>[4,5]</sup>, suggesting that the Al-4.4Mg alloy 5083 might also exhibit sufficient formability for the ISC process. Successful flow forming of a 5xxx-series alloy with acceptable service properties could eliminate the added time and risk of distortion from heat treatment, further capitalizing on the manufacturing rate benefits of the ISC process.

### Flow Forming

Flow forming is an axisymmetric, incremental bulk forming process. Rollers plastically deform material against a rotating mandrel to reduce the workpiece wall thickness and grow the length of the cylinder<sup>[6]</sup>. The integral stiffeners of the ISCs are formed as the rollers force material into grooves machined into the mandrel. Flow forming is commonly used for fabricating steel clutch housings at the 200 mm scale and smooth-walled steel cylinders for the Ariane 5 rocket boosters at the 3 m scale<sup>[7]</sup>. Figure 1 shows the interior of the WF VUD-600 vertical forming machine at NASA Langley Research Center with the major components noted.



Figure 1: WF VUD-600 vertical flow forming machine with main components labeled.

### Formability

Formability is a measure of a material's ability to plastically deform as a function of temperature and stress state. A material's formability is evaluated differently depending on the product form being assessed, e.g. forging evaluations often use the compression test while stamping operations may use a hydraulic bulge test<sup>[8,9]</sup>. Although a universal formability screening test for flow forming does not exist, Bylya et al. have shown that flow formability of steel, Ti, and Al may correlate with tensile behavior<sup>[10]</sup>. The specific properties include work hardening coefficient ( $n$ ), percent area reduction ( $\%AR$ ), and modulus of resilience ( $U_r$ ).

In this study, mechanical testing and exploratory forming trials were conducted to gain an understanding of the ambient temperature formability of three Al rolled plate products: 6061, 2139, and 5083.

## Materials and Methods

### Flow Forming Trials

Pathfinder forming trials were conducted on a WF VUD-600 vertical forming machine at NASA Langley Research Center (Figure 1). Disc-

shaped preforms with an outer diameter of 220 mm, an inner diameter of 50 mm, and thicknesses of 9.5 to 10 mm were used for the forming trials. The preforms were comprised of alloys 6061, 2139, and 5083 in the annealed (fully soft) condition. Alloys 6061 and 2139 are medium- and high-strength heat treatable alloys, respectively, while Al 5083 is a work hardenable alloy. Table 1 details the nominal compositions of the three alloys.

Table 1: Nominal compositions of the three Al alloys in this study [11,12].

Element	2139	5083	6061
Ag	0.4	--	--
Cu	5.0	--	0.28
Cr	--	0.15	0.2
Fe	$\leq 0.15$	$\leq 0.4$	$\leq 0.7$
Mg	0.5	4.4	1.0
Mn	0.4	0.7	--
Si	$\leq 0.1$	$\leq 0.4$	0.6
Al	bal.	bal.	bal.

The forming trials utilized the VUD-600 demonstration part geometry provided by the equipment manufacturer. Part formation comprises multiple operations:

- spin forming to convert the disc-shaped preform to a cup-shaped part in five passes;
- forward flow forming to reduce the wall thickness, increase the length, and form the gear teeth;
- reverse flow forming to further thin the smooth-walled portion; and
- hub forming to form the necked-in region.

Figure 2 illustrates the sequence of steps leading to the conversion of a flat plate preform into a fully formed part.

The various forming operations of the VUD 600 machine are combined to create a single G-code program. Unique to a particular part geometry, the same program was employed for all of the trials in this study. The specific rates of forming varied between the spin and flow forming steps. The spindle rotation speed was set between 400-450 rpm. The roller rotation speed was set to 180 rpm prior to part contact and was subsequently accelerated by contact with the spinning part. The roller feed rate varied from 1500 mm/min (spin



Figure 2: Conversion of a disc-shaped preform to a demonstration part through: spin forming, forward flow forming and gear tooth formation, reverse flow forming, and hub forming.

forming) down to 400 mm/min (flow forming). The roller geometry consisted of a diameter of 235 mm, a nose radius of 10 mm, and a shoulder radius of 70 mm. The two rollers were mounted at 45° to the horizontal for the forming trials. The part was cooled at the roller contact points via the impingement of a water-based coolant.

Successful part formation depends on a number of forming outcomes, including:

- dimensional conformance to the intended final part,
- absence of macroscale defects such as cracks, wrinkles, and tears,
- absence of microstructural defects such as void formation around constituent particles, and
- as-formed mechanical properties that include moderate ductility retention.

These criteria were applied to formed parts to assess the forming success of each alloy.

### Tensile Testing and Metallurgical Analysis

Tensile testing of the annealed alloys was performed on the screw-driven MTS Alliance RT/100 universal testing machine shown in Figure 3a and conformed to ASTM E8. The crosshead speed was held constant at 0.0085 mm/s to achieve strain rates on the order of  $10^{-4} \text{ s}^{-1}$ . Strain was measured through visual image correlation (VIC) using the setup shown in Figure 3. Two 5 MP cameras were focused on the test area, and images were collected at a frequency of 1 Hz with a 40 ms exposure time. Rectangular tensile specimens with a 6.35 x 6.35 x 31.75 mm gage region were machined via wire electrical discharge machining (EDM) and used for testing. Specimens were

oriented along the rolling direction (L) of the plate to measure the preform properties. The samples were painted on the camera-facing side with a thin layer of flat white spray-paint, followed by flat black spray-paint speckles to establish the pattern for VIC. Three virtual extensometers of 25.4 mm length were applied to the gage region of the sample and averaged to extract longitudinal strain (Figure 3b). At least two specimens were tested for each alloy.

Analysis of the fracture surfaces of the tensile specimens and failed parts was performed in a Hitachi S-3700N scanning electron microscope (SEM). Measurements to compute %AR were taken of the failed tensile samples using Vernier calipers and conformed to ASTM E8.

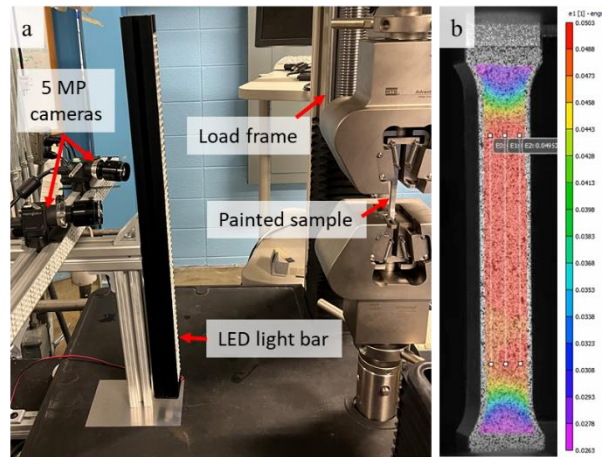


Figure 3: (a) Tensile testing setup, (b) Speckle-painted sample with VIC results displayed at 5% strain.

## Results

### Pathfinder Forming Trials

Figure 5a shows the results of the forming trials. Al 6061 demonstrated sufficient formability to conform to the intended part geometry without any macroscale defects, consistent with prior work showing the alloy's high flow formability in parts up to the 3 m scale<sup>[13]</sup>. However, further work is needed to assess its complete success with respect to microstructural characteristics and as-formed mechanical properties. In contrast, both Al 2139 and Al 5083 failed during the third spin forming pass in the conversion of the disc-shaped preform to a flanged cylinder. Examination of the Al 5083 fracture surface in the SEM (Figure 5b) confirmed that the Al 5083 part failed in shear at the bend

between the tailstock clamping region and the developing walls of the spun-formed cup.

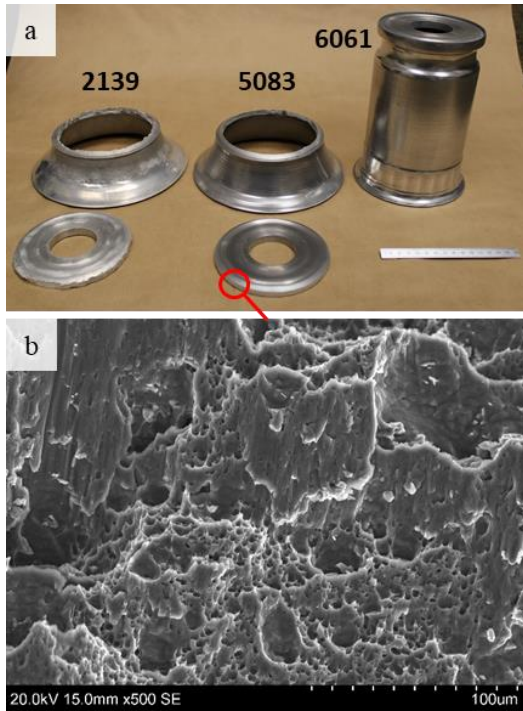


Figure 5: Results of the pathfinder forming trials, (a) Al 2139 and Al 5083 only partially formed, whereas Al 6061 was fully formed into a demonstration part. (b) Fracture surface of the Al 5083 part showing shear failure during the third spin forming pass.

### Tensile Properties

The results from ASTM E8 tensile tests are shown in Figure 4 and detailed in Table 2. The engineering stress-strain curve of Al 6061 is significantly lower than those of Al 2139 and Al 5083, demonstrating lower strength in the annealed condition. The 6061 alloy also exhibits 30% higher total elongation (strain at failure,  $e_{tot}$ ), indicating greater ductility. The uniform elongation (the amount of strain prior to the peak of the stress-strain plot, i.e. specimen necking) is similar among the three alloys. The 5083 material exhibited significant flow serration compared to the heat treatable alloys, which can be attributed to the Portevin-Le Chatelier (PLC) effect in solid solution-strengthened materials<sup>[14]</sup>.

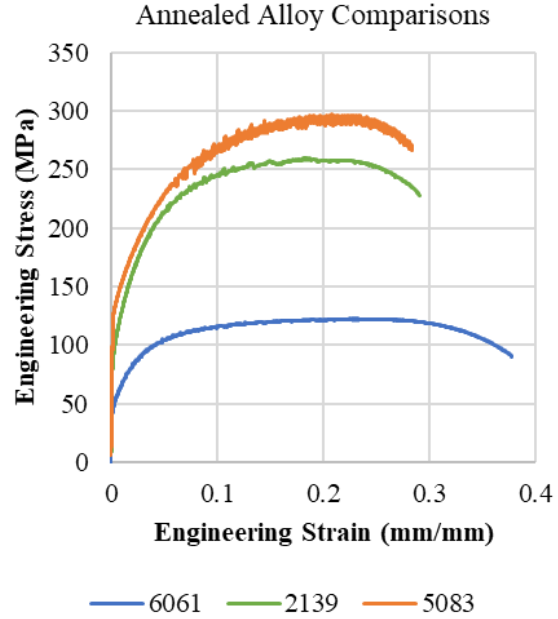


Figure 4: L-direction tensile properties for Al alloys 6061, 2139, and 5083.

Table 2: Average tensile properties of the annealed Al preform materials in the L direction.

	6061	2139	5083
Yield strength (MPa)	48	99	133
Ultimate tensile strength (MPa)	122	260	298
Uniform elongation, $e_{unif}$ (%)	22.2	17.1	21.0
Total elongation, $e_{tot}$ (%)	36.7	27.9	28.7
Area reduction, %AR (%)	62	38	36
Work hardening coefficient, $n$	0.25	0.31	0.29
Modulus of resilience, $U_r$ ( $\times 10^6$ J/m <sup>3</sup> )	0.11	0.25	0.37
Modulus of toughness, $U_t$ ( $\times 10^6$ J/m <sup>3</sup> )	45.0	63.2	75.0

Another significant point of departure for the 6061 alloy was its high %AR, which was 60% greater than those of alloys 2139 and 5083. The

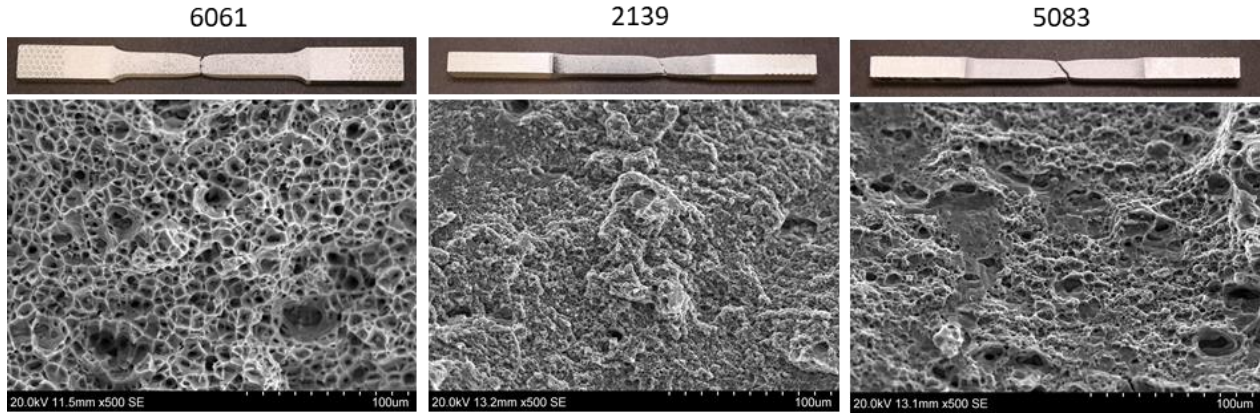


Figure 6: SEM and optical images of the failed tensile specimens ; (a) Al 6061 exhibited ductile tensile fracture with large dimples and a fracture surface normal to the loading axis; (b) & (c) Al 2139 and Al 5083 exhibited 45° fracture plane, as well as shear features and fine dimples on the fracture surface.

6061 tensile samples also demonstrated a different fracture morphology, with a greater necked region resembling ductile cup-and-cone fracture. In contrast, the 2139 and 5083 materials failed in 45° shear fracture. Figure 6 shows the macroscopic fracture morphology of the three alloys and the associated microscopic fracture features in the SEM. The Al 6061 fracture characteristics comprised comparatively large, ductile dimples in the center of the sample while the Al 2139 and Al 5083 fracture surfaces showed regions of shallow dimples and smeared shear fracture features.

Three additional parameters were calculated from the stress-strain results. The first is the work hardening coefficient,  $n$ , which is calculated by fitting the uniform plastic portion of the true stress-true strain ( $\sigma_T$ - $\varepsilon_T$ ) curve with Equation 1:

$$\sigma_T = K\varepsilon_T^n \quad (1)$$

where  $\sigma_T$  and  $\varepsilon_T$  are calculated from the engineering stress and strain ( $\sigma_E$  and  $\varepsilon_E$ ) via Equations 2 and 3.

$$\sigma_T = \sigma_E(1 + \varepsilon_E) \quad (2)$$

$$\varepsilon_T = \ln(1 + \varepsilon_E) \quad (3)$$

The modulus of resilience,  $U_r$ , is the measure of storable elastic energy of the material.  $U_r$  was calculated by integrating the elastic region of the curve (e.g. from  $\varepsilon_E = 0$  through the strain at the yield stress). Similarly, the modulus of toughness,  $U_t$ , was calculated by integrating over the entire stress-strain curve. Thus,  $U_t$  represents the total energy that can be absorbed by the material

before failure. These parameters, combined with the %AR, were suggested by Bylya et al.<sup>[10]</sup> to be measures of flow formability.

### Discussion

Premature failure of Al 2139 and Al 5083 during spin forming occurred in a similar manner despite being from differing alloy families. Note that alloys 2139 and 5083 are precipitation- and solid solution-strengthened, respectively. The results from this study suggest that three parameters caused the greatest impact on alloy performance –  $n$ , %AR, and  $e_{tot}$ . The work hardening coefficient is a measure of the rate of strength increase accompanying strain accumulation during part deformation. It is surmised that the repetitive working of the material at the tailstock clamping region caused localized regions of high work hardening. Figure 8 consists of frames from a video of Al 6061 being formed without coolant and demonstrates the progressive working of the material near the tailstock clamping region. This localized work hardening likely elevated the strength in that region at the expense of ductility, leading to increasingly brittle behavior during subsequent passes. High tensile stresses would have developed at the tailstock clamping region during the third downward spin forming pass, creating microcracks and voids in a region of already high damage accumulation from work hardening. As a consequence of the relatively low %AR and  $e_{tot}$  during tensile deformation of Al 2139 and Al 5083 compared to Al 6061, the parts failed in shear shortly after reaching ultimate strength.



Figure 8: Image series showing the progressive spin forming steps for Al 6061. The final image shows the point of failure for alloys 2139 and 5083.

In contrast, the 6061 material exhibited a lower work hardening coefficient (revealed by the flattened tensile curve in Figure 4) than the other alloys. This lower  $n$  allows the material to deform without significant hardening, leading to slowed strain hardening in the tailstock clamping region. The high  $\%AR$  and  $e_{tot}$  of Al 6061 allowed the material to deform after reaching ultimate strength and even extend to higher thickness reductions without failure.

Certain tensile properties such as  $U_r$  and  $n$  did not correlate with formability as suggested in the literature<sup>[10]</sup>. This is probably due to the Al 2139 and Al 5083 failures occurring prior to the flow forming step, suggesting that other material characteristics may have correlated with *spin* formability. An assessment of the relevancy of  $U_r$  and  $n$  for predicting *flow* formability will be deferred until the spin forming failures are resolved.

An Al 5083 spin forming trial was performed to investigate the tailstock clamping region prior to failure. The program was interrupted after the second downward spin forming pass, i.e. the third frame in Figure 8. A cross section extracted from the part revealed that the part had thinned in the same location where the Al 2139 and Al 5083 parts failed during the third spin forming step. Figure 7 shows the interrupted Al 5083 part and its cross section. The smaller cross sectional area would have driven failure to that region, and the downward forces from the third spin forming pass would have encouraged vertical shear failure. This result suggests that future spin forming pass designs should attempt to minimize thinning in the tailstock clamping region to promote more even distribution of stresses.

Other measures will likely be needed to suppress the premature failures in Al 5083 and Al 2139 besides spin forming pass schedule. One possible solution is intermediate annealing, where forming is paused prior to failure and the part is

subjected to a one hour 350-400°C thermal treatment and a slow cool<sup>[15]</sup>. Annealing reverses the effects of work hardening, restores the original properties of the material, and allows for further deformation without fracture. Intermediate annealing could also be implemented after the final spin forming pass so that the flow formability could be studied without the effect of work hardening.

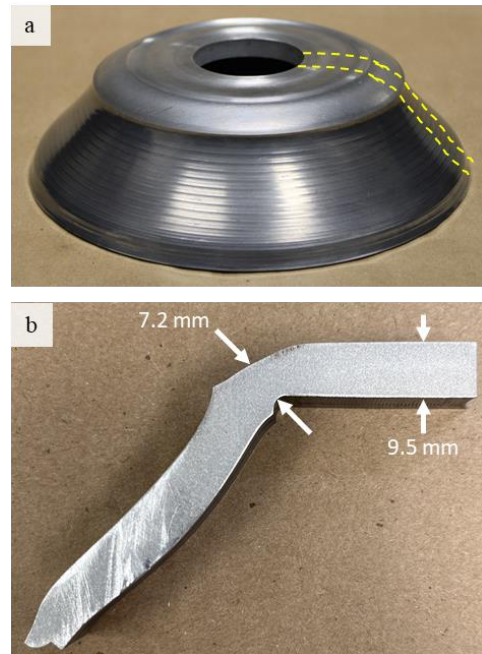


Figure 7: (a) Al 5083 part interrupted after the 2nd downward spin forming pass. (b) Cross section from the part in (a) showing a thinned region where the shear failure of prior parts occurred.

## Conclusions

This investigation reveals that multiple mechanical properties can contribute to the forming success of Al alloys. The following conclusions are drawn:

1. The Al 6061 alloy exhibited excellent spin and flow formability due to its higher

starting ductility and tendency towards ductile fracture over shear.

2. Al 2139 and Al 5083 exhibited very similar failures during spin forming in spite of differing alloy families.
3. The Al 5083 part exhibited shear failure in the tailstock clamping region due to the localized thinning in concert with vertical tensile stresses.
4. Spin formability correlated with the  $n$ ,  $\%AR$ , and  $e_{tot}$  values derived from tensile testing. Al 2139 and Al 5083 (high  $n$ , low  $\%AR$ , and low  $e_{tot}$ ) failed prematurely. Al 6061 (15% lower  $n$ , 60% higher  $\%AR$ , and 30% higher  $e_{tot}$ ) formed completely.

### Future Work

There are a number of key thrusts that will be pursued to advance this project. So far, flow formability evaluations at NASA and in the literature have focused on uniaxial tensile testing. The next steps in the coupon-scale formability testing will include compression tests to assess compressive fracture strength and morphology. Notched tensile tests will also be explored to probe higher triaxiality stress states, which have been shown to cause failure in flow forming<sup>[10]</sup>. The results from the three formal test methods will be compiled into forming limit diagrams for the three alloys and create a basis for future formability screening of new alloys.

Research on the VUD-600 will seek to standardize forward flow formability trials, rather than simply assessing the quality of parts at the conclusion of forming. The flow formability trials will determine the maximum thickness reduction capability of each alloy. This approach will provide

a quantitative measure of formability that can be compared to the results from the mechanical testing to determine the best predictive measures. Improvements in the spin forming pass design will be implemented to increase uniformity in the wall thickness at the tailstock clamping region. Intermediate annealing trials between critical spin forming passes will also be conducted to restore the formability of Al 2139 and Al 5083. These modifications will enable stable formation of cylindrical preforms with high formability for the flow forming trials.

Finally, metallurgical analysis and mechanical testing will be conducted on the as-formed parts to study the impacts of the flow forming process on as-formed strength and residual ductility. It is anticipated that the 5083 alloy will exhibit competitive as-formed properties, eliminating the need for heat treatment. This will enhance the potential of the ISC process as an efficient manufacturing method for aerospace structures.

### Acknowledgments

The authors gratefully acknowledge the NASA Advanced Air Transport Technology (AATT) program and the Virginia Space Grant Consortium (VSGC) for the funding of this work. Thanks also to Harold Claytor and Joel Alexa of the Advanced Materials and Processing Branch (AMPB) at NASA LaRC for their assistance in the flow forming trials, and to Wes Tayon and Dave Stegall of the AMPB for their collaboration on the tensile testing. Special thanks to Dr. James Fitzgerald at UVA and Karen Taminger of NASA LaRC for their mentorship during this research.

## References

- [1] E.K. Hoffman, A.K. Boddorff, K.M. Taminger, C. Mulvaney, D.E. Stegall, Advanced Lightweight Metallic Fuselage Project Manufacturing Trade Study, NASA Technical Memo 2021-0026758. (2022). <https://ntrs.nasa.gov/citations/20210026758>.
- [2] M.C. Stoner, A.R. Hehir, M.L. Ivanco, M.S. Domack, Cost-Benefit Analysis for the Advanced Near Net Shape Technology (ANNST) Method for Fabricating Stiffened Cylinders, NASA Technical Memo 2016-219192. (2016). <https://ntrs.nasa.gov/citations/20160006525>.
- [3] W.A. Tayon, M.S. Domack, J.A. Wagner, Characterization of 10-ft. Diameter Aluminum Alloy 2219 Integrally Stiffened Cylinders, NASA Technical Memo 2019-220260. (2019). <https://ntrs.nasa.gov/citations/20190002739>.
- [4] M. Haghshenas, R.J. Klassen, Mechanical characterization of flow formed FCC alloys, *Materials Science and Engineering: A*. 641 (2015) 249–255. <https://doi.org/10.1016/j.msea.2015.06.046>.
- [5] M. Haghshenas, J.T. Wood, R.J. Klassen, Investigation of strain-hardening rate on splined mandrel flow forming of 5052 and 6061 aluminum alloys, *Materials Science and Engineering: A*. 532 (2012) 287–294. <https://doi.org/10.1016/j.msea.2011.10.094>.
- [6] M. Runge, *Spinning and Flow Forming: Spinning and Flow Forming Technology, Product Design, Equipment, Control Systems, Leifeld Metal Spinning*, 1994.
- [7] D. Zell, M. Domack, W. Tayon, M. Stachulla, J. Wagner, Developments on Low Cost Manufacturing Methods for Cylindrical Launch Vehicle Structures, in: 67<sup>th</sup> International Astronautical Congress, Washington DC, USA, 2019.
- [8] G.E. Dieter, Bulk Workability Testing, in: *ASM Handbook Volume 8: Mechanical Testing*, Fourth Printing, ASM International, 1992: pp. 571–597.
- [9] B. Taylor, Sheet Formability Testing, in: *ASM Handbook Vol. 8 : Mechanical Testing*, 9th ed., ASM International, 1985.
- [10] O.I. Bylya, T. Khismatullin, P. Blackwell, R.A. Vasin, The effect of elasto-plastic properties of materials on their formability by flow forming, *J. Mater. Process. Technol.* 252 (2018) 34–44. <https://doi.org/10.1016/j.jmatprotec.2017.09.007>.
- [11] Aluminum Association, *Aluminum Standards and Data*, Aluminum Association, New York, 2017.
- [12] Aerospace Material Specification AMS4468 : Aluminum Alloy, Plate, 5.0Cu - 0.4Mn - 0.5 Mg - 0.4 Ag (2139-T84), Solution Heat Treated, Cold Worked, and Artificially Aged, (2017). <https://doi.org/10.4271/AMS4468>.
- [13] W.A. Tayon, M.T. Rudd, M.S. Domack, M.W. Hilburger, Development of Advanced Manufacturing Approaches for Single-Piece Launch Vehicle Structures, NASA Technical Memo 2021-0026743. (2022).
- [14] W.J. Poole, J.D. Embury, D.J. Lloyd, Work hardening in aluminium alloys, in: R. Lumley (Ed.), *Fundamentals of Aluminium Metallurgy : Production, Processing, and Applications*, Elsevier Science & Technology, 2010: pp. 307–344.
- [15] Aerospace Material Specification AMS2770R : Heat Treatment of Wrought Aluminum Alloy Parts, (2020). <https://doi.org/10.4271/AMS2770R>.